

# Nonlinear Dynamics Analysis of a Parametrically Resonant MEMS Sensor

Wenhua Zhang, Rajashree Baskaran and Kimberly L. Turner  
Department of Mechanical and Environmental Engineering, EII 2355  
University of California at Santa Barbara, CA 93106-5070  
whzh@engineering.ucsb.edu Fax: (805) 893-8651, Tel (805) 893-7849

## 1. ABSTRACT

Novel mass sensors based on parametric resonance can achieve high sensitivity because of the sharp transition from zero to large response. Unlike harmonic resonance based mass sensors, the sensitivity of this novel class of sensors will not be affected by damping. However, the presence of nonlinearity in the spring and electrostatic force of the oscillator significantly change the behavior of parametric resonance. In this paper, a nonlinear Mathieu equation is used to examine the effects of nonlinearity. A two-variable method is utilized to analyze this equation. The effects are validated by experiments.

## 2. INTRODUCTION

Many MEMS based mass sensors detect mass changes by measuring shifts in resonance frequency. To implement high sensitivity, micro-scale oscillators are promising due to their small mass and high quality factor. Some cantilever mass sensors have been developed and been applied as chemical sensors, biosensors and other sensors as well [1-3]. We have previously introduced the framework of designing a novel parametrically driven mass sensor with higher sensitivity than normal cantilever sensor [4]. Here, we present a detailed analysis and experimental verification of effects of cubic nonlinearity on a parametrically driven MEMS oscillator. The presence of nonlinearity in recovery spring and electrostatic force alters the dynamic behavior of parametric resonance dramatically.

In the case of harmonic oscillator with time-modulated stiffness, parametric resonance exists at some specific frequency [5]. The transition from zero response (stable state) to large response (unstable state) can be very sharp [6]. In a torsional oscillator, 0.001Hz has been observed in experiment [6]. Since the transition frequency depends on system parameters, including mass, small mass change in this system can be detected by measuring the shift of transition frequency. The novel mass sensing system consists of a mechanical oscillator, with electrostatic actuator and sensor. A special comb finger configuration actuates the oscillator and tunes the stiffness of the system as well. When a square root AC voltage is applied on the actuator, the first parametric resonance can be excited at ~twice the natural frequency.

The smallest detectable mass change depends on transition step size and parameters of system and electrical signal

( $dm \propto d\omega/\omega^3$ ,  $\omega \sim 2\omega_0$ ). To improve the system sensitivity, higher stiffness and smaller mass is warranted. Signal-to-noise ratio is another important issue in sensor design. To be able to obtain good signal, larger amplitudes are desired, implying that nonlinearity in spring and electrostatic force cannot be ignored.

## 3. THERORETICAL ANALYSIS

### 3.1 DEVICES

The device we have studied is an oscillator, which was designed by Adams for the independent tuning of linear and cubic stiffness terms [7]. It is fabricated using SCREAM process [8]. A Scanning Electron Micrograph of the oscillator is shown in Figure1. The device covers about  $500 \times 400 \mu\text{m}^2$ . It has two sets of parallel interdigitated comb finger banks on either end of the backbone and two sets of non-interdigitated comb fingers on each side. The four folded beams provide elastic recovery force for the oscillator. The beams, backbone and the fingers are ~2 microns wide and ~12 microns deep. Either the interdigitated or the non-interdigitated comb fingers may be used to drive the oscillator. In this study, non-interdigitated comb fingers are used to drive the oscillator.

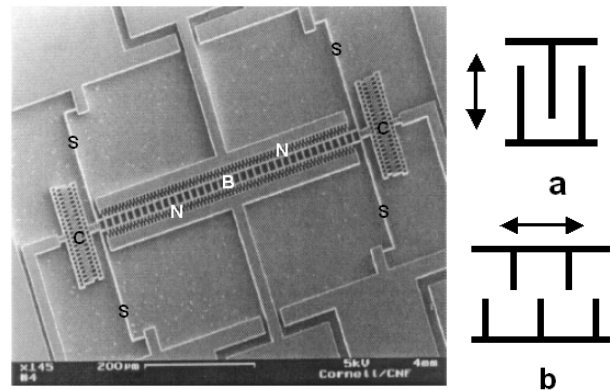


Figure 1: A Scanning Electron Micrograph of the oscillator. Note the folded beam springs (S), the two sets of interdigitated comb finger banks (C) on both end of backbone (B) and non-interdigitated comb fingers (N) on each side of backbone (B). Figure 1(a) and (b) are schematic of interdigitated comb fingers and non-interdigitated comb fingers.

### 3.2 ANALYSIS

Using Newton's laws, the 1-D motion of the device can be described by the following equation:

$$m \frac{d^2 x}{dt^2} + c \frac{dx}{dt} + F_r(x) = F_e(t, x) \quad (1)$$

where  $x$  is displacement,  $m$  is mass and  $c$  is damping.

Considering nonlinearity, the recovery force can be expressed as:  $F_r(x) = k_1 x + k_3 x^3$  (2)

where,  $k_1$  and  $k_3$  are linear stiffness and cubic stiffness respectively.

When a square root AC voltage signal ( $V = (\cos(\omega t))^{1/2}$ ) being applied on the non-interdigitated comb fingers,  $F_e$  is a function of displacement  $x$  and time  $t$  [7].

$$F_e(x, t) = -(r_1 V_A^2 x + r_3 V_A^2 x^3) \cos(\omega t) \quad (3)$$

Substituting  $F_e$  and  $F_r$  in equation (1) and normalizing it:

$$\frac{d^2 x}{d\tau^2} + \alpha \frac{dx}{d\tau} + (\beta + 2\delta \cos 2\tau)x + (\delta_3 + \delta_3' \cos 2\tau)x^3 = 0 \quad (4)$$

$$\text{where } \alpha = \frac{2c}{m\omega}, \quad \beta = \frac{4(k + r_1 V_A^2)}{m\omega^2}, \quad \delta = \frac{2r_1 V_A^2}{m\omega^2},$$

$$\delta_3 = \frac{4k_3 + 4r_3 V_A^2}{m\omega^2}, \quad \delta_3' = \frac{4r_3 V_A^2}{m\omega^2}$$

This is a nonlinear Mathieu Equation. All the terms in this equation except  $\beta$  (which is of order 1) is of small order. Hence, we can use perturbation methods to study this system. By assuming  $\delta = \varepsilon$ ,  $\beta = \beta_0 + \varepsilon\beta_1$ , the equation can be rewritten as a harmonic oscillator with a perturbation (the terms on the right hand side).

$$\frac{d^2 x}{d\tau^2} + \beta_0 x = \varepsilon [-(\beta_1 + 2\cos 2\tau)x + (\gamma_3 + \gamma_3' \cos 2\tau)x^3 - \mu \frac{dx}{d\tau}] \quad (5)$$

where the terms in equation (5) have been scaled with respect to the small term  $\varepsilon$ ,

$$\gamma_3 = \frac{\delta_3}{\varepsilon}, \quad \gamma_3' = \frac{\delta_3'}{\varepsilon}, \quad \mu = \frac{\alpha}{\varepsilon}$$

We know that for a linear Mathieu equation, the first order parametric resonance occurs when the driving frequency is near twice the resonant frequency (here that would correspond to  $\beta_0=1$ ). So, we use the 'method of two variable expansion' [9] to analyze the equation when driving near the first parametric resonance. The idea of the method is that the expected solution involves two time scales: the time scale of the periodic motions and a slower time scale that modulates the amplitude of the periodic motion. Here, we use the notation that  $\xi$  represents stretched time ( $\xi = \omega t$ ), and  $\eta$  represents slow time ( $\eta = \varepsilon t$ ) [9]. Assuming  $x = x_0 + \varepsilon x_1$  and  $\beta = 1 + \varepsilon\beta_1$  and using the two variable expansion method, the equation of motion can be rewritten as two equations:

$$4 \frac{\partial^2 x_0}{\partial \xi^2} + x_0 = 0 \quad (6)$$

$$4 \frac{\partial^2 x_1}{\partial \xi^2} + x_1 = -4 \frac{\partial^2 x_0}{\partial \xi \partial \eta} - (\beta_1 + 2\cos \xi)x_0 - (\gamma_3 + \gamma_3' \cos \xi)x_0^3 - 2\mu \frac{\partial x_0}{\partial \xi} \quad (7)$$

It should be noted that we are working with first order expansion and  $O(\varepsilon^2)$  terms are neglected here.

The solution to the harmonic oscillator in  $x_0$  is as follows,

$$x_0 = A(\eta) \cos\left(\frac{\xi}{2}\right) + B(\eta) \sin\left(\frac{\xi}{2}\right) \quad (8)$$

Unlike, the simple harmonic oscillator case, we have the "constants"  $A$  and  $B$  varying in slow time. Using this solution to evaluate the right hand side of the equation in  $x_1$  and setting the condition for removal of the resonant terms, yields the 'slow-flow' equations in  $A$  and  $B$  (the dynamics of  $A$  and  $B$  in slow-time).

$$\frac{dA}{d\eta} = -\frac{\mu}{2}B + \frac{B}{2}(\beta_1 - 1) + \frac{3B\gamma_3}{8}(A^2 + B^2) - \frac{\gamma_3' B^3}{4} \quad (9)$$

$$\frac{dB}{d\eta} = -\frac{\mu}{2}A - \frac{A}{2}(\beta_1 + 1) - \frac{3A\gamma_3}{8}(A^2 + B^2) - \frac{\gamma_3' A^3}{4} \quad (10)$$

The characteristics of these two equations are schematically shown in A-B plane, see figure 3(a). The plane can be divided into three areas. In area I, one center exists at (0,0) which means only one stable trivial solution exists in the area. In area II, there are two centers at ( $\pm a_1, 0$ ) and one saddle at (0,0), corresponding to one stable nontrivial solution and one unstable trivial solution. In area III, there are two centers at ( $\pm a_2, 0$ ), two saddles at (0,  $\pm b$ ) and one center at (0,0), corresponding to one stable nontrivial solution, one unstable nontrivial solution and one stable trivial solution.

For clarity of discussion, we present the influence of damping and nonlinear term on parametric resonance separately.

#### 3.2.1 Effect of Damping (assuming no cubic nonlinearity)

Equation (9,10) can be simplified as

$$\frac{dA}{d\eta} = -\frac{\mu}{2}B + \frac{B}{2}(\beta_1 - 1) \quad (11)$$

$$\frac{dB}{d\eta} = -\frac{\mu}{2}A - \frac{A}{2}(\beta_1 + 1) \quad (12)$$

From Equations (11, 12), the transition curve from stable to unstable areas in the first parametric resonance can be found [9]:

$$\beta = 1 \pm \varepsilon \sqrt{1 - \mu^2} = 1 \pm \sqrt{\varepsilon^2 - \alpha^2} \quad (13)$$

#### 3.2.2 Effect of cubic nonlinearity (assuming no damping)

We look at the slow flow equations in polar coordinates here, and assume  $A = R \cos \theta$  and  $B = R \sin \theta$ . Equation (9) and (10) can be modified as:

$$\frac{dR}{d\eta} = -\frac{R}{2} \sin(2\theta) \quad (14)$$

$$\frac{d\theta}{d\eta} = -\frac{\beta_1}{2} - \frac{3\gamma_{3\text{eff}} R^2}{8} - \frac{1}{2} \cos(2\theta) \quad (15)$$

where  $\gamma_{3\text{eff}} = \gamma_3 + \frac{2\gamma_3'}{3} \cos(2\theta)$  is defined as effective nonlinear parameter.

We study the equilibrium (fixed) points of the slow-flow variable ( $R^*$ ,  $\theta^*$ ) and analyze their stability characteristics. The equilibrium points are when the right hand side of the above equations is identically zero. For non-trivial solutions of  $R$ , equilibrium points are

$$\theta^* = 0, \frac{\pi}{2}, \pi, \frac{3\pi}{2} \text{ and}$$

$$R^2 = -\frac{4}{3\gamma_{3eff}}(\beta_1 + \cos(2\theta^*)) \quad (16)$$

Let us assume effective nonlinearity parameter  $\gamma_{3eff} < 0$ . In the case of  $\theta^* = 0$  and  $\pi$ ,  $R^2 = -\frac{4}{3\gamma_{3eff}}(\beta_1 + 1)$ , nontrivial

solutions require  $\beta_1 > -1$ . When  $\theta^* = \frac{\pi}{2}$  and  $\frac{3\pi}{2}$ ,

$$R^2 = -\frac{4}{3\gamma_{3eff}}(\beta_1 - 1), \text{ nontrivial solutions exist only for } \beta_1 > 1.$$

The characteristics of equation (16) are schematically shown in Figure 3(b). Since  $\beta_1 = \pm 1$  corresponds to transition curves from stable to unstable areas in  $\beta$ - $\delta$  plane, bifurcation occurs when we quasi-statically vary frequency of the input voltage across the transition curve. The growth of  $R^*$  with respect to  $\beta$  in different areas is schematically shown in figure 3(b), where solid line represents stable solution and dashed line represents unstable solution.

#### 4. EXPERIMENTAL VERIFICATION

A multi-dimensional MEMS motion characterization suite is used to measure the in plane movement of the device [10]. The device is placed in a vacuum chamber, where the pressure can be pumped to as low as 7mTorr. The motion is measure using a Laser Doppler Vibrometer through an optical microscope.

A square root AC voltage signal is applied on the non-interdigitated comb fingers. By sweeping the driving frequency around twice the natural frequency, the frequency response of the first parametric resonance can be captured. Figure 4 is a velocity response of the device with driving voltage  $V_A = 20V$ . The frequency is swept from low to high and high to low. Different step sizes are used in the sweeping. When sweeping the frequency from high to low, the device becomes unstable at about 52.7kHz. But when sweeping from low to high, the jump from unstable to stable occurs around 53.7kHz. And this jumping point depends on the step size of frequency. The smaller the step size, the larger the transition frequency (points S and R).

#### 5. DISCUSSION

According to the analysis of Nonlinear Mathieu equation, first order parametric resonance as represented in the  $\beta$ - $\delta$  plane (which translates to  $V_A$ - $\omega$  coordinates) may be categorized into three areas, I, II and III, see figure 3. The corresponding  $A$ - $B$  plane is shown in the same figure and shows stability characteristics. In area I, only one trivial solution exists. As the frequency is changed quasi-statically, a bifurcation occurs at the left boundary ( $\beta = 1 + \delta$ ). In area II, the trivial solution becomes unstable and simultaneously a stable sub-harmonic motion is born. This motion grows in amplitude as  $\delta$  increases. In the right boundary ( $\beta = 1 - \delta$ ), the unstable trivial solution becomes stable again and an unstable sub-harmonic motion is born. The stable sub-harmonic nontrivial solution born in area II also exists in area III.

The experimentally obtained displacements exactly verify all the characteristics expected from the analysis. Figure 4 presents typical frequency response in the three zones described above. In area I, the response is very small, which is a stable trivial solution. In area II, a large response exists,

corresponding to the stable nontrivial solution, while the unstable trivial solution cannot be found. In area III, one large and one small response can be found, corresponding to one stable trivial solution and one stable nontrivial solution, while the unstable nontrivial can not be observed. Analysis predicts that, depending on the initial displacement and velocity, the final displacement converges to one of the two stable states. When sweeping frequency from high to low, the initial value will be small and hence the trivial stable solution is obtained. But when sweeping the frequency from low to high, in small step sizes, the response will stabilize at the nontrivial stable solution.

As we keep increasing the driving frequency, the large response will jump to zero at some frequency beyond the right transition boundary. Sweeping the driving frequency with different sep sizes, the jump point can be different. For large step size sweeps, the response jumps to the trivial stable solution at a lower frequency, see point R in figure 4. If we sweep the driving frequency with very small steps, the jump will happen at a higher frequency, see point S in Figure 4. We theorize that the step size causes a perturbation in the initial conditions, thereby affecting the frequency at which the jump occurs. It is worthwhile to note here that, the difference in response between sweeping driving frequency in either direction (increasing or decreasing values) is due to the bifurcations occurring at the boundaries. This response appears like a system "hysteresis", but in fact is a distinctly different dynamic behavior.

The jump is very critical in the application as a mass sensor. To sweeping driving frequency in different manners, many jumps can be observed. For most of the jumps, the frequency where jump happens depends more on sweeping manners than system parameters. However, only one jump happens at the right transition boundary when we sweep the driving frequency from high to low. The jump point is very stable and depends only on the system parameters. This implies that to detect mass changes, we must sweep driving frequency from high to low in our case ( $\gamma_{3eff} < 0$ ).

One distinguishing feature of parametrically driven mass sensor is that the sensitivity is independent of damping. The presence of damping alters the shape of the transition curve (from 'V' to 'U'), but the sharp transition still exists, even in the air. From the analysis and experimental results, we note that the effect of the damping in the system is to shift the instability 'tongue' from one that looks like a 'V' to one that looks like a 'U', see figure 3. This implies that there's a minimum input voltage above which the transition will take place. The damping does not affect the sensitivity of the mass sensor, but just introduces a constraint to the input voltage signal amplitude, unlike the sensors based on detecting natural frequency shifts, such as normal cantilever sensors. This is a very critical feature of the sensor since often the quality factor cannot be controlled with precision or made very large in test situations.

#### 6. CONCLUSION

This work presents theoretical analysis and experimental tests of nonlinear effects on parametric resonance. As shown by theory, presence of structural and electrostatic nonlinearity in a MEMS oscillator changes the behavior of parametric resonance significantly. These effects are

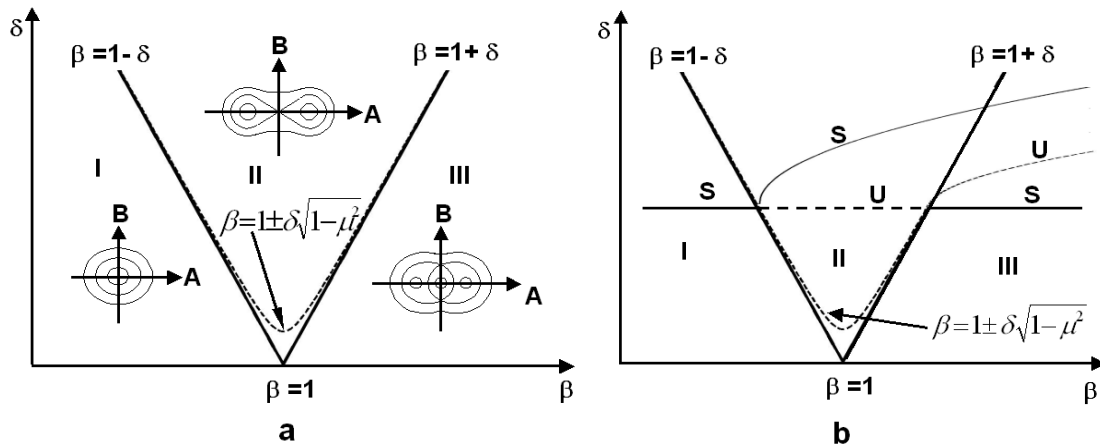


Figure 3 Dynamic characteristics of Nonlinear Mathieu Equation in the  $\beta$ - $\delta$  plane.  $\beta=1\pm\delta$  are the transition curves, which divide  $\beta$ - $\delta$  plane into area I, II, III. Note the damping effects on transition curves ( $\beta=1\pm\delta\sqrt{1-\mu^2}$ ) in figure 3 (a). The number of stable points change in each area - one center at (0,0) in area I, two centers at  $(\pm a_1, 0)$  and one saddle at (0,0) in area II, three centers at  $(\pm a_2, 0)/(0,0)$  and two saddles at  $(0, \pm b)$  in area III. Figure 3(b) shows how the positions of the stable and unstable points vary as  $\beta$  and  $\delta$  are varied quasi-statically.

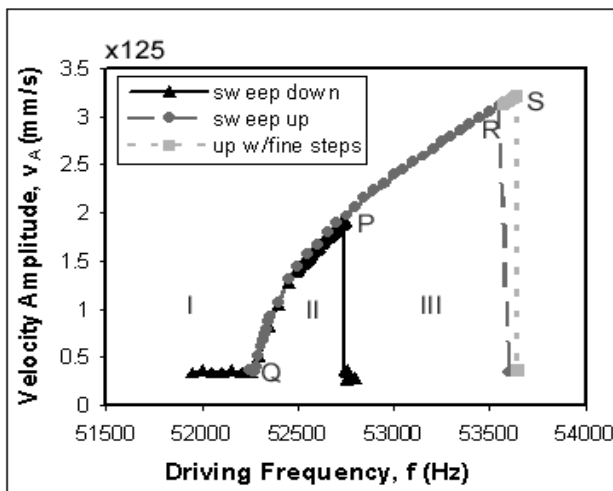


Figure 4 Experimental data of frequency-amplitude curves as the input frequency is swept quasi statically near first order parametric resonance (twice the natural frequency and  $\beta=1$ ) at  $V_A=20$  V. The figure can be divided into three areas, I, II and III (Refer figure 3 for the distinction). Point P is in the right transition curve ( $\beta=1+\delta$ ) from area II to I and Q is in the left transition curve ( $\beta=1-\delta$ ) from area III to II. Note there are two experimental responses in area III, corresponding to the two stable solutions. The points R and S are in region III where the response jumps from the large amplitude stable response to the trivial solution.

validated by experimental results. Based on the analysis and experiments, an appropriate working mode for this type of mass sensor is found. The sensitivity of the novel mass sensor will be nearly independent of damping. To improve the sensitivity, new design and fabrication are underway.

## 7. ACKNOWLEDGMENT

The authors would like to thank Scott Adams for the device fabrication.

## 8. REFERENCE

- [1] Lang, H. P., Berger, R., Battiston, F., Ramseyer, J. P., Meyer, E., Andreoli, C., Brugger, J., Vettiger, P., Despont, M., Mezzacasa, T., Scandella, L., Guentherodt, H. J., Gerber, C. and Gimzewski, J. K., A chemical sensor based on a micromechanical cantilever array for the identification of gases and vapors, p.S61-64,
- [2] Fritz, J., Baller, M. K., Lang, H. P., Rothuizen, H., Vettiger, P., Meyer, E., Guntherodt, H. J., Gerber, C. and Gimzewski, J. K., Translating biomolecular recognition into nanomechanics, Science (USA), 288 (5464), p.316-318, 2000.
- [3] Thundat, T., Wachter, E. A., Sharp, S. L. and Warmack, R. J., Detection of mercury vapor using resonating microcantilevers, Appl. Phys. Lett. (USA), 66 (13), p.1695-1697, 1995.
- [4] Turner, K. L. and Zhang, W., Design and analysis of a dynamic MEM chemical sensor, Proceedings of the 2001 American Control Conference, Arlington, VA, USA, p.1214-1218 vol.1212, 25-27 June 2001.
- [5] Turner, K. L., Miller, S. A., Hartwell, P. G., Macdonald, N. C., Stogartz, S. H. and Adams, S. G., Five parametric resonances in a microelectromechanical system, Nature (UK), 396 (6707), p.149-152, 1998.
- [6] Turner, K. L., Hartwell, P. G., Bertsch, F. M. and Macdonald, N. C., Parametric resonance in a microelectromechanical torsional oscillator, ASME International Mechanical Engineering Congress and Exposition Proceedings of Microelectromechanical Systems (MEMS), Anaheim, CA, USA, p.335-340, 15-20 Nov. 1998.
- [7] Adams, S. G., Bertsch, F. M., Shaw, K. A. and Macdonald, N. C., Independent tuning of linear and nonlinear stiffness coefficients [actuators], J. Microelectromech. Syst. (USA), 7 (2), p.172-180, 1998.
- [8] Macdonald, N. C., SCREAM microelectromechanical systems, Microelectron. Eng. (Netherlands), 32 (1-4), p.49-73, 1996.
- [9] Rand, R. H., Lecture Notes on Nonlinear Vibrations, <http://www.tam.cornell.edu/randdocs/>,
- [10] Turner, K. L., Hartwell, P. G., Macdonald, N. C., Multi-Dimensional MEMS Motion Characterization Using Laser Vibrometry, Transducers'99, Sendai, Japan, 7-10 June, 1999.